analytical chemistry

Article

Cite This: Anal. Chem. 2018, 90, 8600−8606

pubs.acs.org/ac

Tunable, Sheathless Focusing of Diamagnetic Particles in Ferrofluid Microflows with a Single Set of Overhead Permanent Magnets

Qi Chen,[†,‡,⊥] Di Li,[†,⊥] Amirreza Malekanfard,[†] Quanliang Cao,[§] Jianhan Lin,[‡] Maohua Wang,[‡] Xiaotao Han,[§] and Xiangchun Xuan*[,†]

[†]Department of Mechanical Engineering, Clemson University, Clemson, South Carolina 29634-0921, United States

[‡]MOA Key Laboratory of Agricultural Information Acquisition Technology (Beijing), China Agricultural University, Beijing 10083, China

[§]Wuhan National High Magnetic Field Center and State Key Laboratory of Advanced Electromagnetic Engineering and Technology, Huazhong University of Science and Technology, Wuhan 430074, China

Supporting Information

ABSTRACT: There has been increasing interest in the use of magnetic fluids to manipulate diamagnetic particles in microfluidic devices. Current methods for diamagnetic-particle focusing in magnetic fluids require either a pair of repulsive magnets or a diamagnetic sheath flow. We demonstrate herein a tunable, sheathless focusing of diamagnetic particles in a microchannel ferrofluid flow with a single set of overhead permanent magnets. Particles are focused into a single stream near the bottom wall of a straight rectangular microchannel, where a magnetic-field minimum is formed as a result of the magnetization of the ferrofluid. This focusing can be readily switched off and on by removing and replacing the permanent magnets. More importantly, the particle-focusing position can be tuned by shifting the magnets with respect to the microchannel. We perform a systematic experimental study of the parametric effects of the fluid-particle-channel system on diamagnetic-particle focusing in terms of a defined particle-focusing effectiveness.

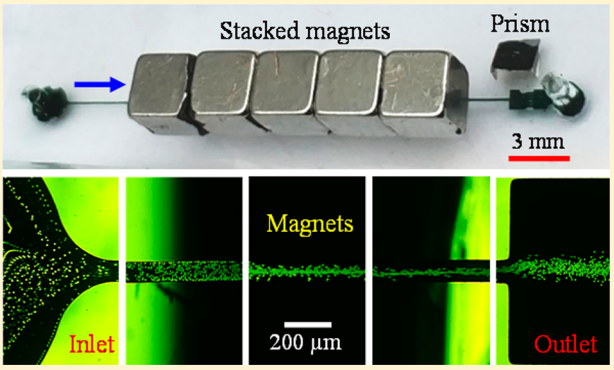

Focusing particles (both biological and synthetic) into a single tight stream is usually a necessary upstream operation in numerous microfluidic applications.[1−4] The most powerful approach to particle focusing is using sheath flows, which can work efficiently for very small particles by simply increasing the flow-rate ratio between the sheath fluid and particle suspension.[5,6] This approach, however, becomes difficult to implement if particles need to be focused in both the horizontal and vertical directions for so-called three-dimensional focusing. Moreover, the use of a large amount of particle-free sheath fluid significantly increases the operating cost and dilutes the particle concentration.[7,8] Therefore, a variety of sheathless particle-focusing approaches have been developed in microfluidic devices, which are classified as either passive or active depending on the source of the involving force.[9] Passive focusing exploits the fluid-flow (e.g., inertial[10−13] or viscoelastic lift[14−17])- or channel-structure (e.g., hydrodynamic filtration[18] and hydrophoresis[19])-induced internal forces to manipulate particles to equilibrium positions. In contrast, active focusing relies on an externally imposed force field (e.g., an acoustic[20] or electric[21] field), other than the force that pumps the particle suspension, to remotely act upon particles and direct them to the position of nil force. The most important feature of active-focusing approaches lies in how easy it is to turn the external force field on and off without affecting the flow of particle suspension itself.

Using a magnetic field to focus particles is relatively new and has not been well developed, although it has clear advantages over other active-focusing approaches, such as its low cost and lack of fluid-heating issues if permanent magnets are used.[22−25] Magnetic focusing of particles has been implemented in the use of magnetophoresis either along (i.e., positive magnetophoresis[26]) or against (i.e., negative magnetophoresis[27]) magnetic-field gradients. The former motion requires particles to be manipulated being magnetizable.[28,29] However, the majority of biological (the only exceptions being red blood cells[30] and magnetotactic bacteria[31]) and synthetic (except magnetic particles) particles are diamagnetic, which must be tagged with one or multiple magnetic particles in order to experience positive magnetophoresis under a nonuniform magnetic field. Therefore, there has been growing interest in using magnetic fluids, which include paramagnetic solutions and ferrofluids, to induce negative magnetophoresis for

Received: April 23, 2018
Accepted: June 20, 2018
Published: June 20, 2018

DOI: 10.1021/acs.analchem.8b01813
Anal. Chem. 2018, 90, 8600−8606

continuous-flow deflection,[32−34] concentration,[35−37] and separation[38−45] of various diamagnetic particles (see the recent review articles from Yang et al.[46] and Zhao et al.[47] as well as the references cited therein).

Magnetic focusing of diamagnetic particles has so far been demonstrated in two primary methods, both of which are three-dimensional because of the inherent magnetic-field gradients of a regular magnetic source (e.g., a permanent or electric magnet) in all dimensions.[48] The first method is to use two repulsive magnets to create a magnetic-field gradient null at their symmetry line, which can be located at either the center or any other lateral position of a microchannel.[49] This design, however, must overcome the repulsion force between the magnets to align them with respect to the flow, which has been implemented by Pamme's group[50,51] using a mechanical setup. Alternatively, Zhu et al.[52] and Zeng et al.[53] embedded permanent magnets directly into the substrate of their microfluidic devices for on-chip focusing. In the second method, Liang and Xuan[54] and Zhou and Wang[55] have each recently demonstrated the use of ferrofluid−water coflows to align magnetically deflected diamagnetic particles along their interface. However, the performance of this sheath-flow magnetic focusing is strongly affected by the diffusive mixing of the two fluids.[55] In a more recent paper Chen et al.[56] used a similar idea to implement the simultaneous separation and washing of diamagnetic particles by size, which results from the integration of negative magnetophoresis and inertial focusing.

We develop in this work a novel, simple method for the tunable, sheathless focusing of diamagnetic particles in a ferrofluid flow through a straight, rectangular microchannel. A single set of stacked permanent magnets are placed directly on top of the microfluidic chip. Hence, they can be readily removed and replaced to switch off and on the magnetic field. The stacked magnets create magnetic-field gradients in both the width and depth directions of the microchannel as a result of the greater magnetization of the ferrofluid than the rest of the microfluidic chip. Diamagnetic particles are focused into a single stream near the bottom wall of the microchannel, whose equilibrium position can be tuned on the fly by shifting the magnets. A systematic experimental study is carried out to understand the effects of various parameters of the fluid−particle−channel system on this diamagnetic-particle focusing.

MATERIALS AND METHODS

Experimental Setup. Figure 1 shows a picture of the microfluidic device. The straight microchannel is 2.4 cm long and has a rectangular cross-section of varying widths and depths. At the end of the channel is a 2 mm long, 900 μm wide expansion for enhanced particle visualization. The microchannel was fabricated with polydimethylsiloxane (PDMS) using a custom-modified soft-lithography method.[57] A right-angle prism (NT32-526, Edmund Optics Inc.) was embedded into the PDMS slab (1 mm thick) and placed 200 μm away from the outlet expansion for visualizing particle motion in the channel-depth direction. Five identical neodymium−iron−boron permanent magnets (B222, 1/8 × 1/8 × 1/8 in., K&J Magnets, Inc.) were stacked together and placed right above the PDMS slab with a symmetric configuration about the microchannel. Three types of spherical, fluorescent, diamagnetic polystyrene particles of 5 μm (Thermo Scientific), 10 μm (Thermo Scientific), and 20 μm (Phosphorex, Inc.) in diameter were each resuspended into a water-diluted EMG 408 ferrofluid (Ferrotec Corporation, the original concentration of magnetic nanoparticles was 1.2 vol %). The particle suspension was driven through the microchannel by a syringe pump (KD Scientific). Particle motions in the channel-width (top view) and -depth (side view) directions were both visualized through an inverted fluorescent microscope (Nikon Eclipse TE2000U, Nikon Instruments) equipped with a CCD camera (Nikon DS-Qi1Mc). The obtained digital images were processed using the Nikon imaging software (NIS-Elements AR 2.30).

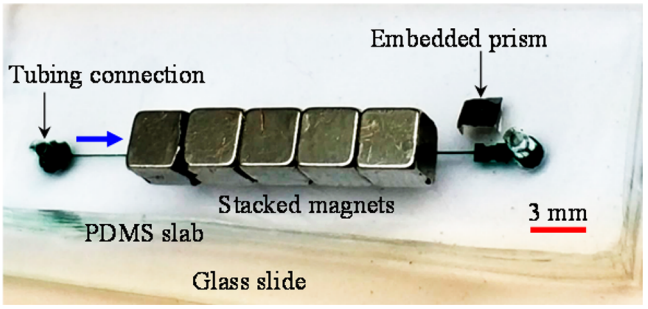

Figure 1. Picture of the microfluidic chip used in the experiments. A prism was embedded into the PDMS slab and placed beside the outlet expansion of the straight, rectangular microchannel for side-viewing. The stacked permanent magnets were placed right above the PDMS slab. The block arrow indicates the flow direction.

Theoretical Analysis. Diamagnetic particles suspended in a ferrofluid experience a negative magnetic force, $\mathbf{F}_M$, and are pushed away from the magnetic source:[57]

$$\mathbf{F}_M = -\frac{1}{6}\pi a^3 \mu_0 (\mathbf{M}_f \cdot \nabla)\mathbf{H} = \frac{1}{12}\pi a^3 \mu_0 \frac{M_f}{H}(-\nabla \mathbf{H}^2) \quad (1)$$

where a is the particle diameter; μ_0 is the vacuum permeability; and $\mathbf{M}_f$ is the ferrofluid magnetization that is collinear with the magnetic field, $\mathbf{H}$, and proportional to the ferrofluid concentration.[58] To achieve sheathless, single-stream focusing of diamagnetic particles in a magnetic-fluid flow, there must exist one magnetic-field minimum over the cross-section of the microchannel. This field minimum is located at the center of the bottom channel wall in our microfluidic chip, which is a result of the dissimilar magnetization of the ferrofluid and the channel substrates. We developed a two-dimensional numerical model to simulate the magnetic field in the cross-sectional plane of the microfluidic chip (see the technical details in the Supporting Information). Figure 2a shows the magnetic-field contour inside and surrounding the microchannel. The magnetization of the ferrofluid significantly distorts the local magnetic field, creating additional magnetic-field gradients in the channel-width direction. The resulting magnetic force on diamagnetic particles is illustrated in Figure 2b using the vector plot of $-\nabla \mathbf{H}^2$ in eq 1. This force directs particles first toward the vertical center-plane and then toward the bottom wall of the microchannel, yielding single-stream focusing. Such sheathless diamagnetic-particle focusing is dependent on the ratio of the transverse magnetophoretic particle velocity, U_M, to the streamwise fluid velocity, U_f:[54]

$$\frac{U_M}{U_f} = \frac{a^2 w h}{Q}\frac{M_f}{H}(-\nabla \mathbf{H}^2)\frac{\mu_0}{36\eta f_D} \quad (2)$$

which is a function of the particle size, a; channel width, w; channel depth, h; ferrofluid flow rate, Q; ferrofluid magnetization, M_f (proportional to the ferrofluid concentration); and

DOI: 10.1021/acs.analchem.8b01813
Anal. Chem. 2018, 90, 8600−8606

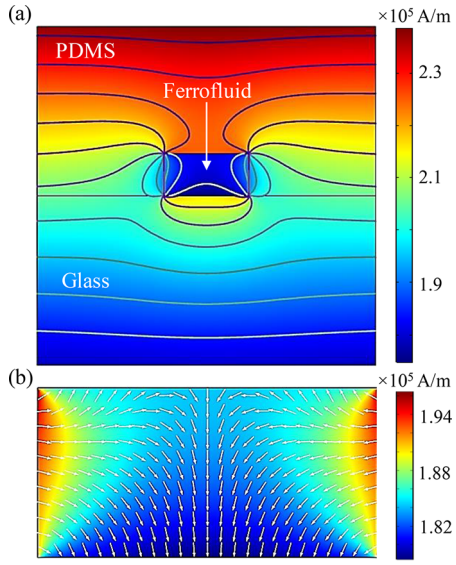

Figure 2. Simulation results in the cross-sectional plane of the microfluidic chip: (a) magnetic-field contour (with contour lines) inside and surrounding the ferrofluid-filled microchannel and (b) ferrofluid-induced-magnetic-force vectors (normalized) on diamagnetic particles, represented by $-\nabla\mathbf{H}^2$ in eq 1, inside the microchannel. The background shows the magnetic-field contour.

magnetic field, H. Other symbols include the ferrofluid viscosity, η, and the wall-induced-drag coefficient, f_D.[57]

RESULTS AND DISCUSSION

Demonstration of Particle Focusing. Figure 3 shows the experimental images of 10 μm in diameter diamagnetic particles in the flow of 0.75× EMG 408 ferrofluid (i.e., 0.75 times the original concentration) through a rectangular, 100 μm wide, 50 μm deep microchannel. The volumetric flow rate is Q = 0.75 mL/h with a calculated Reynolds number of $Re = 2\rho Q/\eta(w + h)$ = 2.78, where ρ is the ferrofluid density. In the absence of the permanent magnets, the particles are uniform everywhere as seen from the lower-row images (both the top and side views) in Figure 3. This indicates a negligible inertial focusing, which itself should direct particles toward two streams in the vertical center-plane of the high-width−depth-ratio (100/50 = 2.0) microchannel.[10,11] This is because the calculated particle Reynolds number, $Re_p = Re(a/D_h)^2$ = 0.06, in the flow is far less than 0.1, where D_h is the hydraulic diameter of the microchannel.[59,60] In contrast, particles experience an apparent focusing along the length of the microchannel when the magnets are present. As illustrated by the top-view images in Figure 3a (top row), 10 μm particles that are still uniformly dispersed at the front edge of the magnets become focused toward the channel centerline by the middle of the stacked magnets. Such a magnetic focusing continues developing until the back edge of the magnets, although it is slightly weakened at the channel outlet because of the local streamline spreading. The side-view image in Figure 3b (upper row) further confirms that particles are focused into a single stream near the bottom wall of the microchannel.

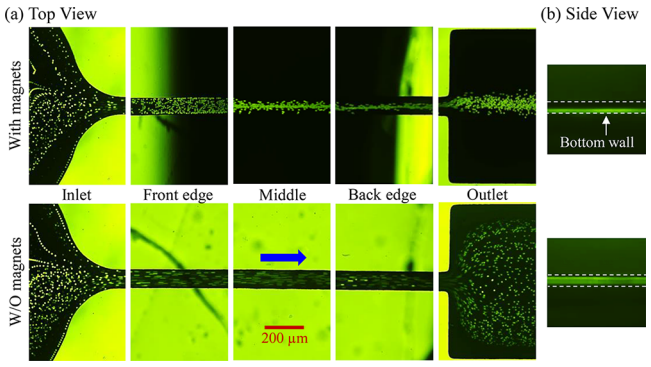

Figure 3. Experimental images of 10 μm diamagnetic particles in the flow of 0.75× EMG 408 ferrofluid through a straight, 100 μm wide, 50 μm deep rectangular microchannel: (a) top-view images at different locations along the channel length and (b) side-view images at the outlet expansion of the channel. The lower dashed-line in each image indicates the bottom channel wall. The images in the upper and lower rows show the results when the stacked permanent magnets (see Figure 1) are present and absent, respectively. The ferrofluid flow rate is fixed at 0.75 mL/h in both cases. The block arrow indicates the flow direction.

Effect of Ferrofluid Flow Rate. Figure 4 (upper row) shows the top-view images of the focusing of 10 μm diamagnetic particles in 0.75× EMG 408 ferrofluid at the channel outlet in a range of flow rates. Particles form a nearly single file line along the channel centerline at the flow rate of 0.1 mL/h, where, as explained above, the inertial effect should not play any role because of the negligible particle Reynolds number (Re_p = 0.008). As predicted from eq 2, increasing the flow rate diminishes the magnetic focusing of the 10 μm particles because their residence time within the effective working region of the magnets is shortened. It is, however, important to note that fluid inertia plays an insignificant role in this decreasing particle focusing over the whole range of flow rates in Figure 4. This is evidenced by the invisible inertial focusing of 10 μm particles in our control experiment (Figure 4, lower-row images), which was carried out under identical experimental conditions except the permanent magnets were removed. This may be due to an insufficient channel length for inertial focusing, even though the particle Reynolds number (Re_p = 0.17) indeed becomes greater than 0.1 at the flow rate of 2.0 mL/h.[59,60]

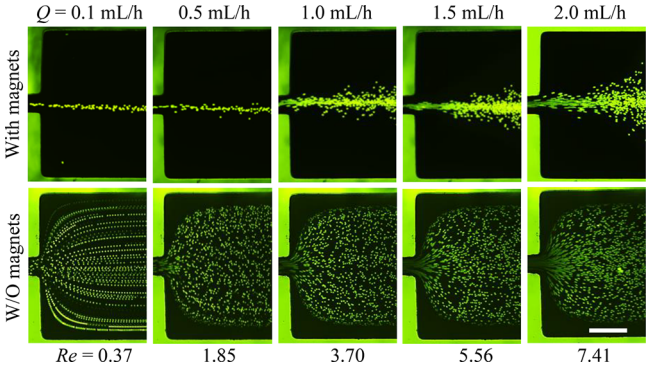

Figure 4. Flow-rate effect on the motion of 10 μm particles in 0.75× EMG 408 ferrofluid at the outlet expansion of a straight, 100 μm wide, 50 μm deep, rectangular microchannel in the presence (top row) and absence (bottom row) of the permanent magnets, respectively. The scale bar represents 200 μm.

Figure 5 presents the experimentally measured stream widths of the focused 10 μm particles at the outlet expansion

DOI: 10.1021/acs.analchem.8b01813
Anal. Chem. 2018, 90, 8600−8606

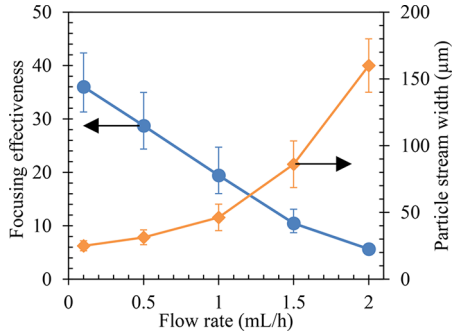

Figure 5. Flow-rate effect on the experimentally measured stream width (from the images in Figure 4) and the calculated focusing effectiveness for 10 μm particles in 0.75× EMG 408 ferrofluid at the outlet expansion of a straight, 100 μm wide, 50 μm deep, rectangular microchannel. Error bars are included to cover the variation of the particle-stream width and hence the focusing effectiveness between the two sets of experimental data.

of the microchannel, which increase from 25 μm at 0.1 mL/h to 160 μm at 2.0 mL/h (more than 5 times). To facilitate a quantitative comparison of diamagnetic-particle focusing in ferrofluids under different working conditions, we define a dimensionless number, focusing effectiveness, to evaluate the particle-focusing performance:

$$\text{focusing effectiveness} = \frac{\text{width of outlet expansion}}{\text{width of the focused particle stream}} \quad (3)$$

where the width of the outlet expansion was fixed at 900 μm in all tests of this work, and the width of the focused particle stream was measured at the edge of the outlet expansion in the experimental images. The plot of the calculated focusing effectiveness versus the ferrofluid flow rate is shown in Figure 5, which exhibits an approximately linear relationship with a negative correlation. This is due to the inverse dependence of diamagnetic-particle deflection (and hence focusing) on the ferrofluid flow rate, as viewed from eq 2.

Effect of Ferrofluid Concentration. Figure 6a compares the top-view images of 10 μm particles in the flows of 1× and 0.5× EMG 408 ferrofluids at the outlet expansion of the microchannel. The particle focusing in the former case is better than that in the lower-concentration ferrofluid at every flow rate. This is because the magnetic force is linearly proportional to the ferrofluid concentration (see eqs 1 and 2). Figure 6b compares the calculated particle-focusing effectiveness in 1×, 0.75×, and 0.5× EMG 408 ferrofluids. Each plot exhibits an approximately linear relationship with respect to the ferrofluid flow rate. Moreover, the value of the particle-focusing effectiveness roughly scales with the ferrofluid concentration for all three flow rates tested: for instance, the focusing effectiveness in the 1× ferrofluid is approximately twice that in the 0.5× ferrofluid. Such a scaling is consistent with the dependence of the induced magnetophoretic particle motion on the ferrofluid concentration. It also remains valid when the magnetic field is varied as a result of, for example, the change in the PDMS thickness (the thicker PDMS, the smaller the magnetic field inside the ferrofluid).

Effect of Particle Size. Figure 7 shows the particle-size effect on diamagnetic-particle focusing in 0.75× EMG 408 ferrofluid at different flow rates. As seen from the top-view

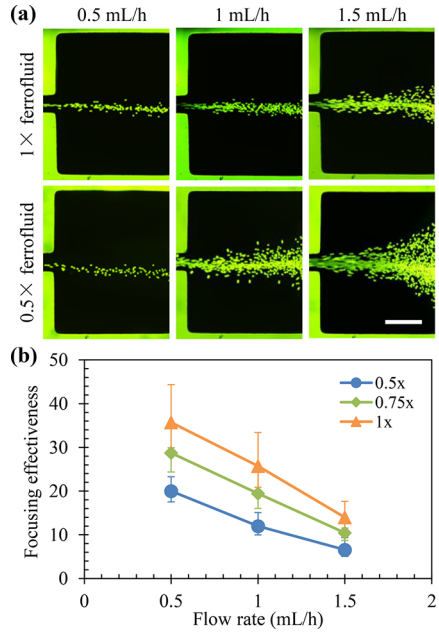

Figure 6. Ferrofluid-concentration effect on the focusing of 10 μm diamagnetic particles in a straight, 100 μm wide, 50 μm deep, rectangular microchannel: (a) top-view images at the outlet expansion in 1× (upper row) and 0.5× (lower row) EMG 408 ferrofluid at different flow rates and (b) plot of the experimentally determined particle-focusing effectiveness (symbols with error bars) vs the ferrofluid flow rate. The scale bar in (a) represents 200 μm.

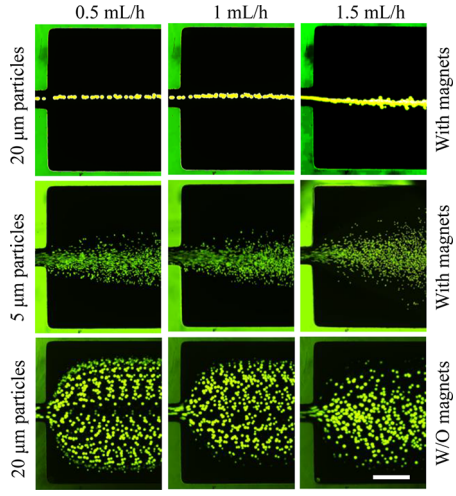

Figure 7. Top-view images of 20 μm (upper row) and 5 μm (middle row) diamagnetic-particle focusing in 0.75× EMG 408 ferrofluid at the outlet expansion of a straight, 100 μm wide, 50 μm deep, rectangular microchannel. The images in the lower row are from a control experiment with 20 μm particles in which all conditions remained the same as those in the upper row except for the absence of the permanent magnets. The scale bar represents 200 μm.

images, 20 μm particles experience significantly better focusing than 5 μm ones and form a nearly single-file stream at the outlet expansion of the microchannel under every flow rate. This phenomenon is apparently due to the particle-volume dependence of the induced magnetic force in eq 1. It is, however, important to note that the contribution of fluid inertia is still insignificant in the test with 20 μm particles. This is evidenced by the observed weak inertial focusing of 20 μm particles at 1.5 mL/h in our control experiment (Figure 7,

DOI: 10.1021/acs.analchem.8b01813
Anal. Chem. 2018, 90, 8600−8606

lower-row images) in which the permanent magnets have been removed. As the particle Reynolds number (Re_p = 0.5) becomes fairly large in this case, we think it is still the insufficient channel length that mitigates the inertial particle focusing.[59,60]

Figure 8 compares the calculated particle-focusing effectiveness of 5, 10, and 20 μm particles versus the ferrofluid flow

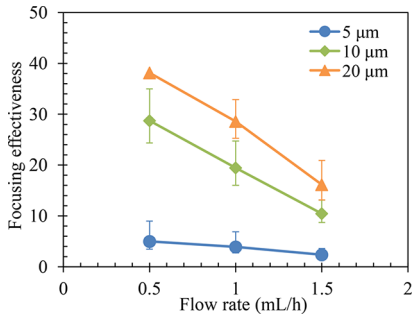

Figure 8. Particle-size effect on the experimentally determined focusing effectiveness (symbols with error bars) in 0.75× EMG 408 ferrofluid at the outlet expansion of a straight, 100 μm wide, 50 μm deep, rectangular microchannel.

rate. Similar to the results of the 10 μm particles in ferrofluids of varying concentrations (Figure 6b), the focusing effectiveness for each type of particle follows a negative linear relationship with respect to the flow rate. Moreover, the focusing effectiveness of the 10 μm particles remains 4−5 times that of the 5 μm particles under all flow rates. This seems consistent with the second-order dependence of magnetophoretic particle deflection in eq 2 on particle size. However, we note that the focusing effectiveness of 20 μm particles is only about 1.5 times that of 10 μm particles under every flow rate. This deviation from the scaling of the particle-size ratio may be attributed to the non-negligible distortion of the 20 μm diamagnetic particles to the magnetic field as well as to the flow field. In future work, we will develop a numerical model to simulate and understand the effects of the dynamic particle−ferrofluid−magnetic-field interactions.

Effect of Microchannel Width. Figure 9a shows the top-view images of the focusing of 10 μm diamagnetic particles in 0.75× EMG 408 ferrofluid at the outlet expansion of 50 and 200 μm wide, straight microchannels. The channel depth is fixed at 50 μm, the same as that in all the above tests. Particles are significantly better focused in 50 μm wide channels than in the wider ones, including both those with 100 μm widths (Figure 4, top row) and those with 200 μm widths (Figure 9a), under the same flow rate. This should be a consequence of the three variations associated with the increase in channel width: the first is the reduced ferrofluid flow speed, which increases the particle response time to magnetic-field gradients and hence facilitates particle focusing; the second is the extended lateral-migration distance, which makes particle focusing more difficult; and the third is the weakened magnetic-field gradients in the channel-width direction, which reduces particle focusing. Figure 9b shows the plots of particle-focusing effectiveness versus the ferrofluid flow rate in the three equal-depth microchannels. Each plot still follows a negative linear relationship, consistent with those presented above. Interestingly, the particle-focusing effectiveness in the 50 μm wide channel is about 1.5 times that in the 100 μm wide channel and 6 times that in the 200 μm wide channel. These values are

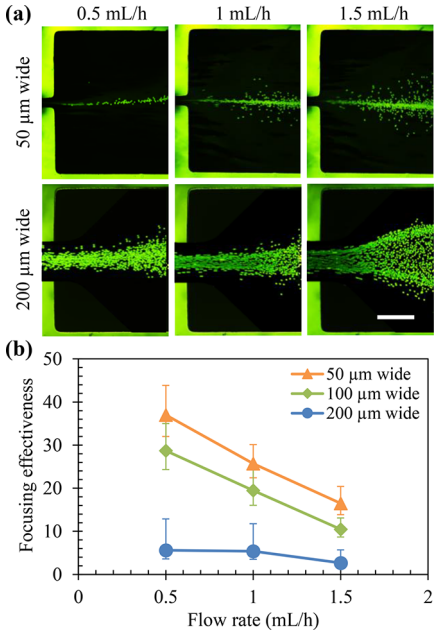

Figure 9. Microchannel-width effect on the focusing of 10 μm diamagnetic particles in 0.75× EMG 408 ferrofluid: (a) top-view images at the outlet expansion of straight, 50 μm-deep microchannels with widths of 50 μm (top row) and 200 μm (bottom row) and (b) experimentally determined particle-focusing effectiveness (symbols with error bars) vs ferrofluid flow rate. The scale bar in (a) represents 200 μm.

not correlated with the channel-width ratio in a simple linear form (as seen in eq 2) because of the competition of the three above-noted variations.

Effect of Microchannel Depth. Figure 10 compares the focusing of 10 μm diamagnetic particles in the flow of 0.75× EMG 408 ferrofluid through 50 μm wide, straight microchannels of different depths. Interestingly, particle focusing is not significantly different when the channel depth is doubled from 50 to 100 μm. This phenomenon may be attributed to the two opposing influences accompanied by the increase of

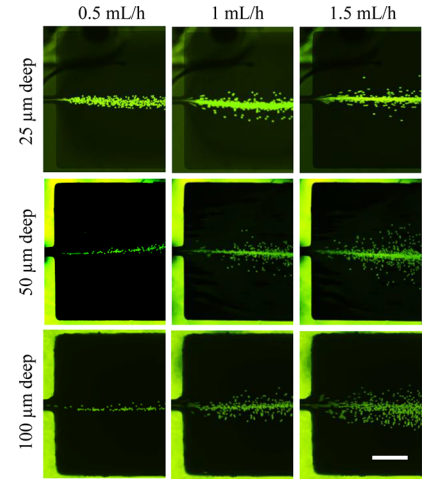

Figure 10. Top-view images of the focusing of 10 μm diamagnetic particles in 0.75× EMG 408 ferrofluid at the outlet expansion of straight, 50 μm-wide microchannels with depths of 25 μm (upper row), 50 μm (middle row), and 100 μm (lower row). The scale bar represents 200 μm.

DOI: 10.1021/acs.analchem.8b01813
Anal. Chem. 2018, 90, 8600−8606

channel depth at the same flow rate: one is the decreased flow speed, which enhances particle focusing, and the other is the decreased magnetic-field gradients, which reduce particle focusing. More interestingly, we notice an enhanced particle focusing in the 25 μm deep channel with the increase of flow rate, although the particle focusing in the two deeper channels still decreased like in all the other tests. The mechanism behind this phenomenon is currently unknown, but it is speculated to be related to the increased confinement in the shallower microchannel. The immediate impacts of confinement may include the increasingly significant distortion of diamagnetic particles to the magnetic and flow fields as well as the increasingly significant redistribution of magnetic nanoparticles in the ferrofluid under the combined action of the magnetic and flow fields.

Figure 11 shows the plots for the focusing effectiveness of 10 μm particles in the three microchannels under different

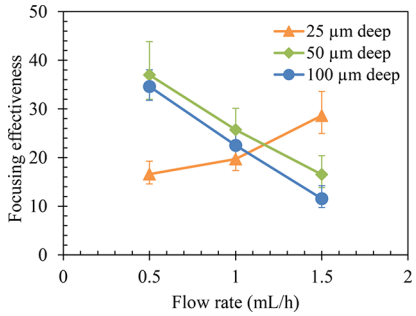

Figure 11. Microchannel-depth effect on the experimentally determined focusing effectiveness of 10 μm diamagnetic particles (symbols with error bars) in the flow of 0.75× EMG 408 ferrofluid through straight, 50 μm wide microchannels.

ferrofluid flow rates. The negative linear line for the 50 μm deep channel is slightly above that for the 100 μm deep channel, but it has a slightly smaller slope. In other words, the particle-focusing effectiveness decreases a little more quickly in the wider channel when the flow rate increases. Interestingly, the plot for the 25 μm deep channel seems to also follow a roughly linear relationship with respect to the flow rate but with a positive slope. A numerical model that considers the full coupling among diamagnetic-particle motion, ferrofluid flow, and magnetic-field distribution will be necessary to understand this abnormal trend observed in the shallowest microchannel.

Effect of Magnet Position. Figure 12 demonstrates the tunable exiting position of the focused 10 μm diamagnetic particles in the flow of 0.75× EMG 408 ferrofluid through a

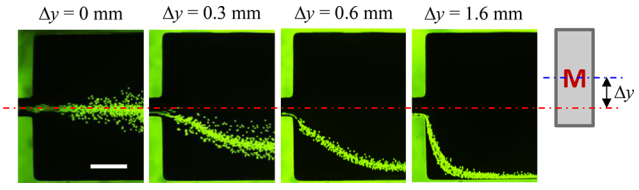

Figure 12. Top-view images of the focusing of 10 μm diamagnetic particles in 0.75× EMG 408 ferrofluid at the outlet expansion when the stacked permanent magnets (see Figure 1) are in line with (i.e., $\Delta y = 0$) or offset from (i.e., $\Delta y > 0$) the channel centerline (see the definition of Δy in the schematic on the right). The straight microchannel is 100 μm wide and 50 μm deep, and the ferrofluid flow rate is fixed at 1.0 mL/h. The scale bar represents 200 μm.

100 μm wide, 50 μm deep microchannel. The flow rate is fixed at 1.0 mL/h. As seen from the top-view images at the outlet expansion, the focused particle stream can be displaced from along the channel centerline to principally any lateral position over the lower half-width of the channel. This is done by simply shifting the stacked permanent magnets (see Figure 1) from being in line with the channel centerline to being offset from it (see the schematic on the right of Figure 12). It is straightforward to suppose that reversing the shifting direction of the magnets should deflect the focused particle stream toward the upper sidewall of the microchannel. This tunable diamagnetic-particle focusing and deflection may potentially be used to achieve targeted particle delivery on the fly. It is apparently a function of ferrofluid flow rate and concentration. It is also expected to depend on particle size, which may enable continuous particle separation and will be studied in our future work.

CONCLUSIONS

We have developed a novel and simple method for three-dimensional diamagnetic-particle focusing in a microchannel ferrofluid flow with a single set of permanent magnets placed on top of the microfluidic chip. This method eliminates the requirement of repulsive magnets or a coflowing sheath fluid, which are used in existing methods, by the use of the inherently formed magnetic-field gradients in the ferrofluid. It offers the flexibility of tuning the particle-focusing position through shifting the magnets relative to the straight microchannel. To understand such a tunable, sheathless diamagnetic-particle focusing, we have conducted a systematic experimental study of multiple parametric effects of the fluid-particle-channel system. We find that the particle-focusing effectiveness increases with increasing ferrofluid concentration or particle size. Moreover, it scales with each of these parameters at a similar scaling to that of the magnetophoretic particle velocity, except for those of the largest particles. The particle-focusing effectiveness also increases as the microchannel width decreases. It follows a negative linear relationship with respect to the ferrofluid flow rate in all these case studies. However, its variation with the microchannel depth is much more complicated, particularly in the shallowest channel with strong confinement effects. We will develop a three-dimensional numerical model to simulate and predict the diamagnetic-particle focusing with full consideration of the dynamic particle−ferrofluid−magnetic-field interactions. We envision that our proposed diamagnetic-particle-focusing method may potentially be used to achieve targeted particle delivery on the fly as well as a continuous-flow particle separation by size.

ASSOCIATED CONTENT

Supporting Information

The Supporting Information is available free of charge on the ACS Publications website at DOI: 10.1021/acs.analchem.8b01813.

Numerical simulation of the magnetic field and ferrofluid-induced magnetic force in the cross-sectional plane of the microfluidic chip (PDF)

AUTHOR INFORMATION

Corresponding Author

*E-mail: xcxuan@clemson.edu. Fax: 864-656-7299.

DOI: 10.1021/acs.analchem.8b01813
Anal. Chem. 2018, 90, 8600−8606

ORCID

Xiangchun Xuan: 0000-0003-0158-4186

Author Contributions

⊥Q. Chen and D. Li contributed equally to this work.

Notes

The authors declare no competing financial interest.

■ ACKNOWLEDGMENTS

This work was supported by the China Scholarship Council (CSC) of the Chinese Government Graduate Student Overseas Study Program (to Q. Chen) and by the NSF under grant CBET-1150670 (to X. Xuan).

■ REFERENCES

(1) Chung, T. D.; Kim, H. C. *Electrophoresis* **2007**, *28*, 4511−4520.
(2) Karimi, A.; Yazdi, S.; Ardekani, A. M. *Biomicrofluidics* **2013**, *7*, 021501.
(3) Jubery, T. Z.; Srivastava, S. K.; Dutta, P. *Electrophoresis* **2014**, *35*, 691−713.
(4) Tang, W.; Tang, D.; Ni, Z.; Xiang, N.; Yi, H. *Anal. Chem.* **2017**, *89*, 3154−3161.
(5) Lu, M.; Ozcelik, A.; Grigsby, C. L.; Zhao, Y.; Guo, F.; Leong, K. W.; Huang, T. J. *Nano Today* **2016**, *11*, 778−792.
(6) Salafi, T.; Zeming, K. K.; Zhang, Y. *Lab Chip* **2017**, *17*, 11−33.
(7) Huh, D.; Gu, W.; Kamotani, Y.; Grotberg, J. B.; Takayama, S. *Physiol Measur.* **2005**, *26*, R73−R98.
(8) Ateya, D. A.; Erickson, J. S.; Howell, P. B., Jr; Hilliard, L. R.; Golden, J. P.; Ligler, F. S. *Anal. Bioanal. Chem.* **2008**, *391*, 1485−1498.
(9) Xuan, X.; Zhu, J.; Church, C. *Microfluid. Nanofluid.* **2010**, *9*, 1−16.
(10) Martel, J. M.; Toner, M. *Annu. Rev. Biomed. Eng.* **2014**, *16*, 371−396.
(11) Liu, C.; Hu, G.; Jiang, X.; Sun, J. *Lab Chip* **2015**, *15*, 1168−1177.
(12) Zhang, Y.; Zhang, J.; Tang, F.; Li, W.; Wang, X. *Anal. Chem.* **2018**, *90*, 1786−1794.
(13) Lee, D.; Nam, S. M.; Kim, J.; Di Carlo, D.; Lee, W. *Anal. Chem.* **2018**, *90*, 2902−2911.
(14) Liu, C.; Ding, B.; Xue, C.; Tian, Y.; Hu, G.; Sun, J. *Anal. Chem.* **2016**, *88*, 12547−12553.
(15) Holzner, G.; Stavrakis, S.; DeMello, A. *Anal. Chem.* **2017**, *89*, 11653−11663.
(16) Del Giudice, F.; Sathish, S.; D'Avino, G.; Shen, A. Q. *Anal. Chem.* **2017**, *89*, 13146−13159.
(17) Asghari, M.; Serhatlioglu, M.; Ortaç, B.; Solmaz, M. E.; Elbuken, C. *Sci. Rep.* **2017**, *7*, 12342.
(18) Aoki, R.; Yamada, M.; Yasuda, M.; Seki, M. *Microfluid. Nanofluid.* **2009**, *6*, 571−576.
(19) Choi, S.; Park, J. K. *Anal. Chem.* **2008**, *80*, 3035−3039.
(20) Jakobsson, O.; Antfolk, M.; Laurell, T. *Anal. Chem.* **2014**, *86*, 6111−6114.
(21) Chen, X.; Ren, Y.; Liu, W.; Feng, X.; Jia, Y.; Tao, Y.; Jiang, H. *Anal. Chem.* **2017**, *89*, 9583−9592.
(22) Pamme, N. *Lab Chip* **2006**, *6*, 24−38.
(23) Zborowski, M.; Chalmers, J. J. *Anal. Chem.* **2011**, *83*, 8050−8056.
(24) Nguyen, N. T. *Microfluid. Nanofluid.* **2012**, *12*, 1−16.
(25) Hejazian, M.; Li, W. H.; Nguyen, N. T. *Lab Chip* **2015**, *15*, 959−970.
(26) Afshar, R.; Moser, Y.; Lehnert, T.; Gijs, M. A. *Anal. Chem.* **2011**, *83*, 1022−1029.
(27) Zhou, Y.; Song, L.; Yu, L.; Xuan, X. *J. Magn. Magn. Mater.* **2016**, *412*, 114−122.
(28) Gijs, M. A. M. *Microfluid. Nanofluid.* **2004**, *1*, 22−40.
(29) Cao, Q.; Han, X.; Li, L. *Lab Chip* **2014**, *14*, 2762−2777.
(30) Zborowski, M.; Ostera, G. R.; Moore, L. R.; Milliron, S.; Chalmers, J. J.; Schechter, A. N. *Biophys. J.* **2003**, *84*, 2638−2645.
(31) Lee, H.; Purdon, A. M.; Chu, V.; Westervelt, R. M. *Nano Lett.* **2004**, *4*, 995−998.
(32) Zhu, T.; Lichlyter, D. J.; Haidekker, M. A.; Mao, L. *Microfluid. Nanofluid.* **2011**, *10*, 1233−1245.
(33) Zhu, J.; Liang, L.; Xuan, X. *Microfluid. Nanofluid.* **2012**, *12*, 65−73.
(34) Tarn, M. D.; Elders, L. T.; Peyman, S. A.; Pamme, N. *RSC Adv.* **2015**, *5*, 103776−103781.
(35) Tarn, M. D.; Peyman, S. A.; Pamme, N. *RSC Adv.* **2013**, *3*, 7209−7214.
(36) Zhou, Y.; Kumar, D. T.; Lu, X.; Kale, A.; DuBose, J.; Song, Y.; Wang, J.; Li, D.; Xuan, X. *Biomicrofluidics* **2015**, *9*, 044102.
(37) Hejazian, M.; Nguyen, N. T. *Biomicrofluidics* **2016**, *10*, 044103.
(38) Zhu, T.; Marrero, F.; Mao, L. *Microfluid. Nanofluid.* **2010**, *9*, 1003−1009.
(39) Shen, F.; Hwang, H.; Hahn, Y. K.; Park, J. K. *Anal. Chem.* **2012**, *84*, 3075−3081.
(40) Vojtisek, M.; Tarn, M. D.; Hirota, N.; Pamme, N. *Microfluid. Nanofluid.* **2012**, *13*, 625−635.
(41) Yan, S.; Zhang, J.; Yuan, D.; Zhao, Q.; Ma, J.; Li, W. *Appl. Phys. Lett.* **2016**, *109*, 214101.
(42) Zhang, J.; Yan, S.; Yuan, D.; Zhao, Q.; Tan, S. H.; Nguyen, N. T.; Li, W. *Lab Chip* **2016**, *16*, 3947−3956.
(43) Zhao, W.; Cheng, R.; Lim, S. H.; Miller, J. R.; Zhang, W.; Tang, W.; Xie, J.; Mao, L. *Lab Chip* **2017**, *17*, 2243−2255.
(44) Zhou, R.; Bai, F.; Wang, C. *Lab Chip* **2017**, *17*, 401−406.
(45) Chen, Q.; Li, D.; Zielinski, J.; Kozubowski, L.; Lin, J.; Wang, M.; Xuan, X. *Biomicrofluidics* **2017**, *11*, 064102.
(46) Yang, R. J.; Hou, H. H.; Wang, Y. N.; Fu, L. M. *Sens. Actuators, B* **2016**, *224*, 1−15.
(47) Zhao, W.; Cheng, R.; Miller, J.; Mao, L. *Adv. Funct. Mater.* **2016**, *26*, 3916−3932.
(48) Han, X.; Feng, Y.; Cao, Q.; Li, L. *Microfluid. Nanofluid.* **2015**, *18*, 1209−1220.
(49) Cao, Q.; Han, X.; Li, L. *J. Phys. D: Appl. Phys.* **2012**, *45*, 465001.
(50) Peyman, S. A.; Kwan, E. Y.; Margarson, O.; Iles, A.; Pamme, N. *J. Chromatography A* **2009**, *1216*, 9055−9062.
(51) Rodriguez-Villarreal, A. I.; Tarn, M. D.; Madden, L. A.; Lutz, J. B.; Greenman, J.; Samitier, J.; Pamme, N. *Lab Chip* **2011**, *11*, 1240−1248.
(52) Zhu, T.; Cheng, R.; Mao, L. *Microfluid. Nanofluid.* **2011**, *11*, 695−701.
(53) Zeng, J.; Chen, C.; Vedantam, P.; Brown, V.; Tzeng, T.-R. J.; Xuan, X. *J. Micromech. Microeng.* **2012**, *22*, 105018.
(54) Liang, L.; Xuan, X. *Microfluid. Nanofluid.* **2012**, *13*, 637−643.
(55) Zhou, R.; Wang, C. *Biomicrofluidics* **2016**, *10*, 034101.
(56) Chen, Q.; Li, D.; Lin, J.; Wang, M.; Xuan, X. *Anal. Chem.* **2017**, *89*, 6915−6920.
(57) Liang, L.; Zhu, J.; Xuan, X. *Biomicrofluidics* **2011**, *5*, 034110.
(58) Rosensweig, R. E. *Annu. Rev. Fluid Mech.* **1987**, *19*, 437−463.
(59) Zhang, J.; Yan, S.; Yuan, D.; Alici, G.; Nguyen, N. T.; Warkiani, M. E.; Li, W. *Lab Chip* **2016**, *16*, 10−34.
(60) Di Carlo, D. *Lab Chip* **2009**, *9*, 3038−3046.

DOI: 10.1021/acs.analchem.8b01813
Anal. Chem. 2018, 90, 8600−8606